Data Repository Item

Supplementary Material

South Atlantic interocean exchange as the trigger for the Bølling warm event

Cristiano M. Chiessi, Stefan Mulitza, André Paul, Jürgen Pätzold, Jeroen Groeneveld, Gerold Wefer

Age model

The age model for core GeoB6211-2 is based on seven accelerator mass spectrometry (AMS) radiocarbon measurements (Leibniz-Laboratory for Radiometric Dating and Stable Isotope Research, Kiel, Germany) (Table DR1, Fig. DR1). Raw radiocarbon dates were calibrated with the CALIB 5.0.2 software (Stuiver and Reimer, 1993) and the Marine04 calibration curve (Hughen et al., 2004).

TABLE DR1. AMS RADIOCARBON DATES AND CALIBRATED AGES USED TO
CONSTRUCT THE AGE MODEL FOR CORE GeoB6211-2

Lab ID	Core depth (cm)	Species	Radiocarbon age ± 1σ error (yr B.P.)	Calibrated age (ka)	2σ calibrated age range (ka)
KIA30528	18	*G. ruber* (pink and white) and *G. sacculifer*	1685 ± 30	1.25	1.30 – 1.16
KIA30527	73	*G. ruber* (pink and white)	7145 ± 55	7.61	7.73 – 7.50
KIA30526	123	*G. ruber* (pink and white) and *G. sacculifer*	12600 ± 70	14.05	14.24 – 13.84
KIA30525	218	*G. ruber* (pink and white) and *G. sacculifer*	13340 ± 80	15.25	15.63 – 14.98
KIA30524	358	Mixed planktic foraminifera*	14860 ± 90	17.40	17.86 – 16.88
KIA30531	448	*Yoldia riograndensis*	15590 ± 100	18.60	18.79 – 18.43
KIA30530	583	*Yoldia riograndensis*	16400 ± 120	19.15	19.43 – 18.96

*Mixed planktic foraminifera contained *G. ruber* (pink and white), *G. sacculifer*, *G. bulloides*, *G. siphonifera*, *T. quinqueloba*, *G. glutinata*, *G. uvula*, *G. conglobatus*, and *G. falconensis*.

The good agreement between measured $\delta^{18}O$ values for *Globorotalia inflata* and *Uvigerina peregrina* averaged for the uppermost 5 cm of GeoB6211-2 (0.94 ‰ and 2.91 ‰, respectively), and the predicted $\delta^{18}O$ of calcite ($\delta^{18}O_{pc}$) (1.02 ‰ and 2.97 ‰, respectively) allowed us to assign modern age to the uppermost cm of GeoB6211-2. We calculated $\delta^{18}O_{pc}$ using seawater $\delta^{18}O$ ($\delta^{18}O_{sw}$) from

LeGrande and Schmidt (2006), temperature from our in situ CTD deployment, and the paleotemperature equation from Shackleton (1974). The depth recorded in the $\delta^{18}O$ of *G. inflata* was assumed to be between 250 m and 300 m. Note that *U. bifurcata* was not available in the uppermost section of the core so we measured *U. peregrina*. Ages between ^{14}C AMS values were linearly interpolated.
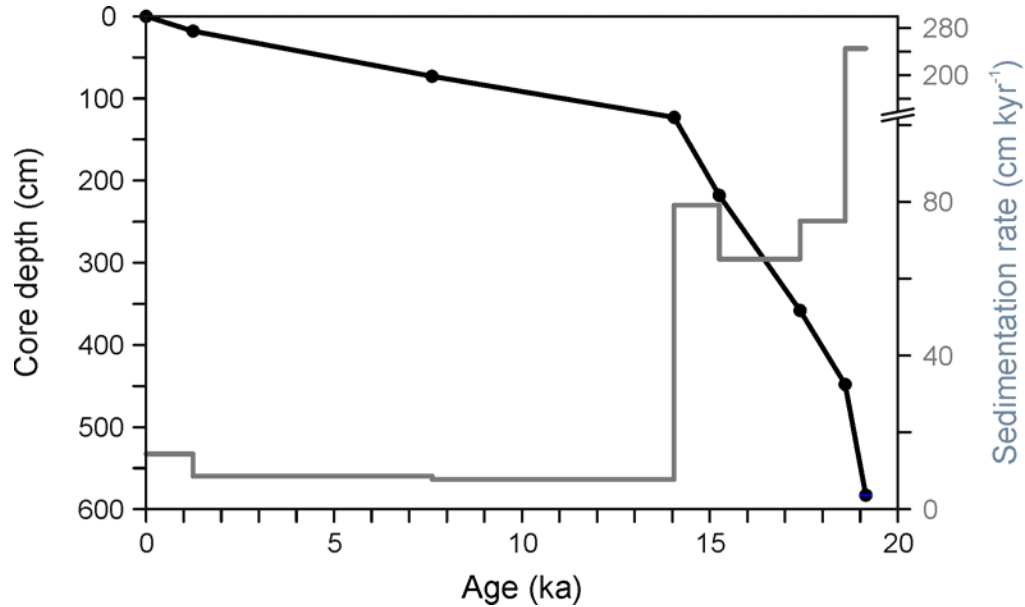

Figure DR1. Age model (black line) and sedimentation rates (gray line) for core GeoB6211-2.

We decided not to apply an additional reservoir age to the two oldest ^{14}C AMS values of our core measured on epibenthic bivalve shells based on two main reasons: (i) $\Delta^{14}C$ measurement from 693 m water depth for GEOSECS station 60 (32.97°S, 42.50°W) (Stuiver and Östlund, 1980), the closest GEOSECS station to our site, when converted to calibrated age using the conventional radiocarbon age equation from Stuiver and Polach (1977), the calibration software CALIB 5.0.2 (Stuiver and Reimer, 1993), and the IntCal04 calibration curve (Reimer et al., 2004) with no reservoir correction results in a value of 470 ± 35 a; this value is close to the 400 yr assigned to the mixed layer at latitudes between 40°N and 40°S (Bard, 1988); at the time of the GEOSECS cruise, bomb-radiocarbon penetration was not deeper than ~450 m for station 60 (Broecker et al., 1995), showing that no bomb-radiocarbon could have lowered the $\Delta^{14}C$ measured value at 693 m water depth at GEOSECS station 60; and (ii) the relatively high velocity (20 m yr^{-1}) of bomb-radiocarbon penetration at around 30°S for central water masses of the South Atlantic as estimated by Broecker et al. (1995) with data from two different

cruises (GEOSECS and SAVE) performed 15 years from each other reflects the relatively quick ventilation of the upper water column at around 30°S in the South Atlantic.

Moreover, the use of questionable corrections in reservoir age for the oldest two bivalve-based calibrated ^{14}C AMS values from our core (18.6 and 19.15 ka) would not change our conclusions, which are grounded on the younger planktic foraminifera-based calibrated ^{14}C AMS values.

We assume no regional deviation from the global reservoir age because the core position lies far from upwelling zones and significantly to the north of the southern polar front. Additionally, the marine reservoir correction database compiled by Reimer and Reimer (2001) shows no data for our site.

Sedimentation rates

Sedimentation rates for GeoB6211-2 show a two-step decrease from the Last Glacial Maximum (LGM) to the Early Holocene (Fig. DR1). Mean values decrease from ~250 to 70 cm kyr^{-1} at around 19 ka and from ~70 to 10 cm kyr^{-1} at around 14 ka. Both changes in sedimentation rates are remarkably synchronous (within age model uncertainties) to outstanding events of sea-level rise related to meltwater pulses (Fairbanks, 1989; Bard et al., 1990; Yokoyama et al., 2000). During the LGM, a ~130 m lower sea-level shifted the coastline very close to our site, especially considering the depth of the shelf break (140 m) in this portion of the Argentine Basin. Submarine channels indicate that the La Plata River extended northwards over the LGM exposed continental shelf (Ewing and Lonardi, 1971; Lonardi and Ewing, 1971). During the LGM, the huge sedimentary load of the La Plata River was directly delivered to the Rio Grande Cone, a major sedimentary feature in the western Argentine Basin where our core was raised. The stepwise rise in sea-level following the LGM caused abrupt displacements of the coastline towards the continent (i.e., away from our site) and trapped a major part of the sedimentary load of the La Plata River in the inner shelf controlling the stepwise decrease in sedimentation rate at our site.

Foraminiferal δ^{18}O and Mg/Ca

The last deglaciation section (from ~90 to 550 cm core depth) of core GeoB6211-2 was sampled at 1 cm intervals for stable oxygen isotope analysis on *G. inflata* (350-500 μm) and *U. bifurcata* (500-650 μm). Taxonomy for identification of benthic foraminifera followed Boltovskoy et al. (1980) and Lutze (1986). For each sample, about 10 and 5 well preserved specimens of *G. inflata* and *U. bifurcata*,

respectively, were analyzed on a Finnigan MAT 252 mass spectrometer equipped with an automatic carbonate preparation device. Isotope results were calibrated relative to the Vienna Peedee belemnite (VPDB) using the NBS19 standard. The standard deviation of the laboratory standard was lower than 0.07 ‰ for the measuring period.

Mg/Ca analyses on *G. inflata* (350-500 µm) were run on a subset of samples with 1-7 cm spacing depending on the sedimentation rate. Fifteen samples distributed around 15 ka were also selected for Mg/Ca analyses on *U. bifurcata* (500-650 µm). For each sample we selected about 20 and 30 well preserved specimens of *G. inflata* and *U. bifurcata*, respectively. Specimens were gently crushed and cleaned following the cleaning protocol of Barker et al. (2003). Dissolved samples were analyzed by ICP-OES (Perkin Elmer Optima 3300 R). Standards (n = 43) and replicate analyses on separate splits of foraminiferal tests (n = 15), which were cleaned and analyzed during different sessions, show mean reproducibility of ± 0.02 and ± 0.09 Mg/Ca mmol/mol, respectively. Each point of Mg/Ca estimate represents an average of three replicate Mg/Ca analyses measured on the same solution and session. Additionally, Fe/Ca, Mn/Ca and Al/Ca ratios were monitored to identify contaminant clay particles and manganese-rich carbonate coatings, which might affect foraminiferal Mg/Ca ratios (Barker et al., 2003). The absence of co-variation between Mg/Ca and Fe/Ca, Mn/Ca and Al/Ca (r^2 < 0.02, for all ratios) attests our Mg/Ca analyses are not biased by contaminants. We converted downcore *G. inflata* Mg/Ca ratios to temperatures using the empirical equation Mg/Ca = 0.831 exp (0.066 T) (r2 = 0.78), based on 25 modern surface samples from the South Atlantic, collected mainly between 20°S and 50°S. To establish the apparent calcification temperatures for our surface samples *G. inflata* Mg/Ca values we first calculated $\delta^{18}O_{pc}$ for the whole water column above every surface sample site by solving the paleotemperature equation from Shakleton (1974) with annual mean temperature data from the World Ocean Atlas 2001 (Conkright et al., 2002) and $\delta^{18}O_{sw}$ from LeGrande and Schmidt (2006). Than, we compared the observed *G. inflata* $\delta^{18}O$ with the respective $\delta^{18}O_{pc}$ profile and established the apparent calcification depth for every *G. inflata* surface sample. These depths were used to extract the apparent calcification temperatures from the World Ocean Atlas 2001 (Conkright et al., 2002). Our *G. inflata* Mg/Ca:temperature calibration equation spans a temperature range from 3°C to 16°C. Details on the Mg/Ca-temperature calibration equation for *G. inflata* will be published elsewhere.

Tilting the isopycnals of the subtropical South Atlantic

The present-day tilt of the isopycnals in a latitudinal transect across the upper South Atlantic at 32.5°S can be observed in Figure DR2. In order to quantify the potential effect that a change in the tilt of the isopycnals would have on the water column properties above our core site we calculated the differences in temperature and $\delta^{18}O_{sw}$ between stations 32.5°S/49.5°W and 32.5°S/15.5°E for every depth of the World Ocean Atlas 2001 (Conkright et al., 2002) and the gridded data set of $\delta^{18}O_{sw}$ from LeGrande and Schmidt (2006) from the surface down to 1500 m water depth (Fig. DR3).
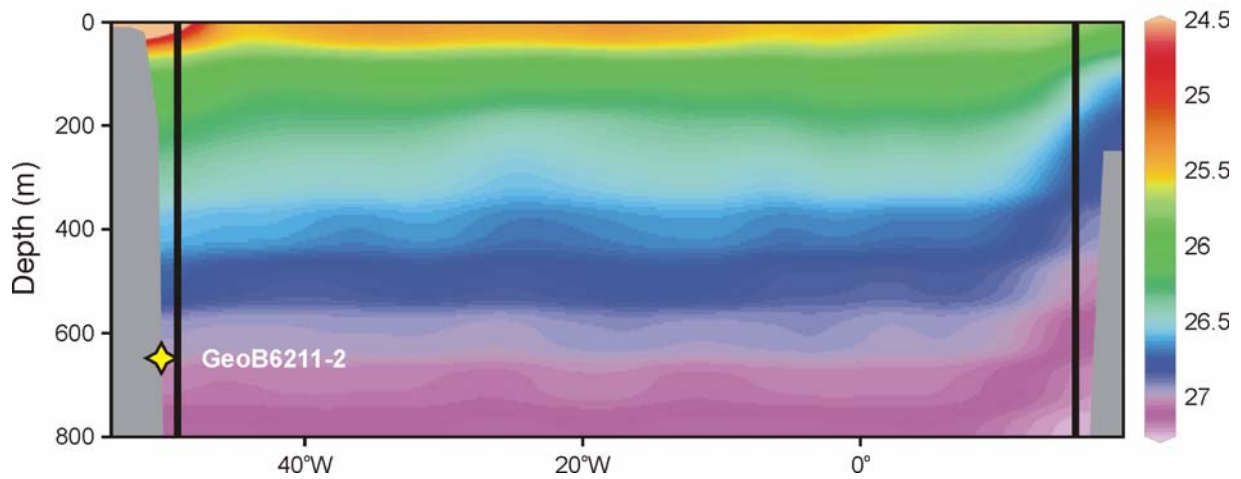

Figure DR2. East-west transect of potential density (referenced to the surface, kg m^{-3}) at 32.5°S across the South Atlantic calculated with data from the World Ocean Atlas 2001 (Conkright et al., 2002). The black vertical lines located at 49.5°W and 15.5°E depict the position of the two stations used in Figure DR3. The yellow star indicates the location of GeoB6211-2.

Freshening of Antarctic Intermediate Water (AAIW) at ~15 ka

Because of the unfavorable signal to noise relation associated to our ice volume corrected bottom seawater $\delta^{18}O$ ($\delta^{18}O_{ivc-bsw}$) reconstruction, the following interpretation of the observed trend in $\delta^{18}O_{ivc-bsw}$ should be treated with caution.

The bottom of the water column at our site shows a decrease in $\delta^{18}O_{ivc-bsw}$ of 0.5 ‰ around 15 ka, clearly opposed to the increase in ice volume corrected permanent thermocline $\delta^{18}O$ ($\delta^{18}O_{ivc-ptsw}$) of ~1.2 ‰ observed for the same period. The apparently contradictory decrease in $\delta^{18}O_{ivc-bsw}$ is actually expected if we consider that: (i) today the conditions recorded by the benthic foraminifera at our site correspond to the boundary between South Atlantic Central Water (SACW) and AAIW where the

influence of relatively warm and salty Indian Ocean waters is rather small; (ii) during the LGM the boundary between SACW and AAIW was even shallower than today so that the bottom conditions at our site were largely controlled by AAIW and the input of cold and fresh waters from the southeastern Pacific Ocean as suggested by modeling results from Paul and Schäfer-Neth (2004); (iii) the strengthening of the Agulhas Leakage was probably related to a synchronous increase of mass transport from the Pacific Ocean into the South Atlantic (Knorr and Lohmann, 2003); and (iv) the abrupt input of isotopically light waters from the melting Patagonian Ice Sheet (PIS) directly to the formation region of AAIW could have decreased its salinity. Modeling results supported by field evidence indeed suggest that the PIS lost ~85% of its volume between 14.5 and 13.7 ka (Hubbard et al., 2005; Turner et al., 2005). Freshening of AAIW would as well intensify North Atlantic Deep Water formation and the Atlantic meridional overturning circulation (AMOC) (Weaver et al., 2003).
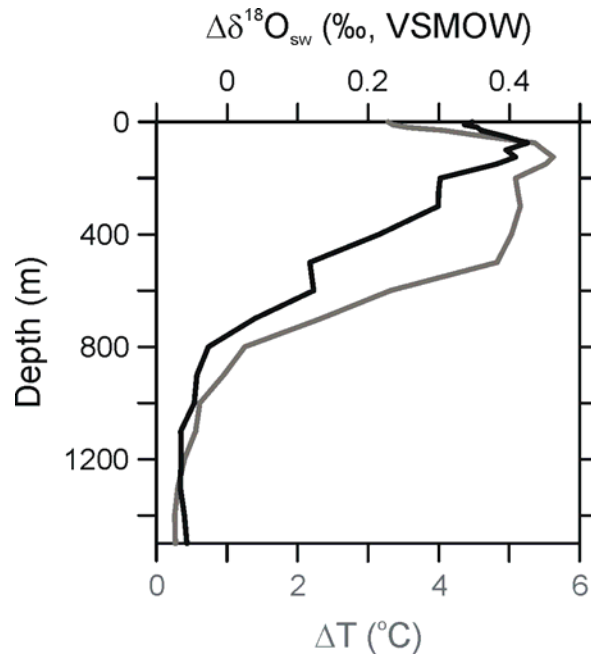

Figure DR3. Depth profiles of the difference in temperature (gray line) and $\delta^{18}O$ (black line) of seawater between two stations located at both extremes (49.5°W and 15.5°E) of a latitudinal transect across the South Atlantic at 32.5°S (Conkright et al., 2002; LeGrande and Schmidt, 2006). The higher differences in the upper water column reflect the northward flowing relatively strong upper branch of the present day Atlantic meridional overturning circulation.

Brief model description, experimental design, results, and discussion

We used the University of Victoria (UVic) Earth System Climate Model (ESCM, version 2.8), which consists of the Modular Ocean Model (MOM, version 2; Pacanowski, 1996) coupled to a vertically integrated two-dimensional energy-moisture balance model of the atmosphere, a sea ice

model (based on the thermodynamic formulation by Semtner (1976) and Hibler (1979) and the dynamic formulation by Hunke and Dukowicz (1997)), a land surface scheme (Cox et al., 1999) and a dynamic global vegetation model (Cox, 2001; Meissner et al., 2003). The UVic ESCM including the atmospheric, ocean and sea ice components is described by Weaver et al. (2001). Monthly wind stress to force the ocean and monthly winds for the advection of heat and moisture in the atmosphere are prescribed from the NCEP reanalysis climatology (Kalnay et al., 1996). The model is driven by the seasonal variation of solar insolation at the top of the atmosphere. The horizontal resolution of the model is constant at 3.6^o in the longitudinal and 1.8^o in the latitudinal direction. There are 19 levels in the vertical, with a thickness ranging from 50 m near the surface to 590 m near the bottom. The vertical levels vary smoothly in thickness, following a parabolic profile. For a systematic comparison of the UVic ESCM climatology with modern observations the reader is referred to Weaver et al. (2001).

We generated two different climate states, one (BL, for Bølling-like) with an active, the other (HL, for Heinrich-like) with a collapsed AMOC. Experiment BL was initialized from a near-equilibrium LGM state with an AMOC reduced by 25%, in terms of the maximum of the meridional overturning streamfunction as compared to a present-day control simulation (~15 vs. ~20 Sv, respectively, 1 Sv = 1×10^6 m^3s^{-1}). Experiment HL was initialized from experiment BL at 17.8 ka and subject to additional freshwater discharge to the North Atlantic Ocean through the St. Lawrence River, at a rate of 0.1 Sv for a period of 100 years. While the LGM experiment was forced by insolation, atmospheric CO_2 concentration and ice sheets fixed at their 21.0 ka values, experiments BL and HL were both forced by changing insolation, atmospheric CO_2 concentration and ice sheets. The wind stress and wind fields in the atmospheric component were allowed to adjust to changes in sea-surface temperature according to a geostrophic wind feedback parameterization (Weaver et al., 2001). In experiment HL, the AMOC totally collapsed. In contrast, experiment BL reached a maximum overturning of ~18 Sv in the year 16.45 ka. In our discussion we compared experiment BL at this stage with experiment HL and thus focused on the difference in ocean temperature due to AMOC collapse.

The strengthening of the AMOC, expressed as the comparison between the BL and the HL climate states, is related to a widespread redistribution of heat in the Atlantic basin (Fig. DR4). Figure DR4A depicts the temperature anomalies (BL – HL) for an east-west transect at 35.1^oS, and Figure DR4B displays the zonally averaged temperature anomalies (again BL – HL) for a north-south transect across the entire Atlantic. Both transects show a dipole-pattern in temperature anomalies that are stronger in the upper ocean (say first 1000 m). Whereas the north-south dipole-pattern in temperature (Fig. DR4B) has been widely discussed (e.g., Crowley, 1992; Manabe and Stouffer, 1997; Rühlemann et al., 2004) we report for the first time an east-west dipole in temperature anomalies at subtropical

latitudes in the South Atlantic (Fig. DR4A). This zonal seesaw seems to be related to a shift in the slope of the isopycnals, that tilt from a flattened position during HL (collapsed AMOC) towards a steepened position during the BL (relatively strong AMOC), generating the warm (cold) anomaly in the western (eastern) South Atlantic. The core of the warming is found between 50 and 500 m water depth, similar to the depth profile of expected temperature change displayed in Fig. DR3. Indeed, the abrupt warming we observed at ~15 ka is higher at the permanent thermocline (6.5°C) compared to the temperature change in the base of the water column (3.5°C).
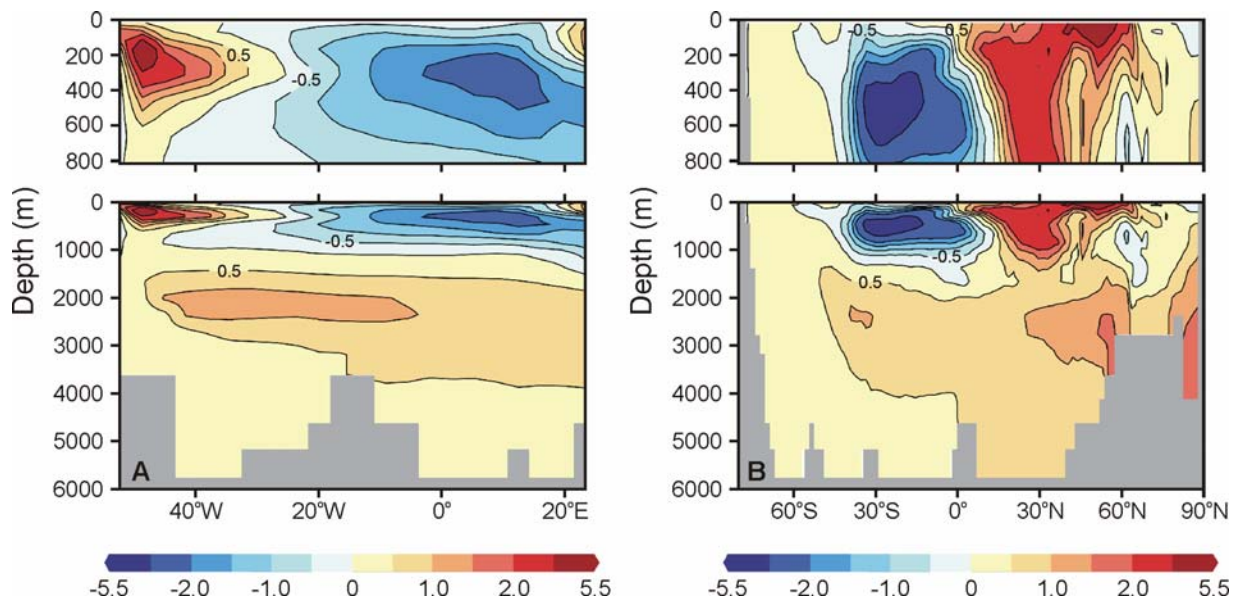

Figure DR4. Temperature anomalies in the Atlantic Ocean between the modeled climate states Bølling-like and Heinrich-like. A: East-west transect of temperature anomalies (Bølling-like – Heinrich-like) at 35.1°S across the South Atlantic. B: Zonally averaged temperature anomalies (Bølling-like – Heinrich-like) for a north-south transect across the entire Atlantic basin.

Supplementary References

Bard, E., 1988, Correction of accelerator mass spectrometry ^{14}C ages measured in planktonic foraminifera: paleoceanographic implications: Paleoceanography, v. 3, p. 635-645.

Bard, E., Hamelin, B., Fairbanks, R.G. and Zindler, A., 1990, Calibration of the ^{14}C timescale over the past 30,000 years using mass spectrometric U–Th ages from Barbados corals: Nature, v. 345, p. 405-410.

Barker, S., Greaves, M., and Elderfield, H., 2003, A study of cleaning procedures used for foraminiferal Mg/Ca paleothermometry: Geochemistry, Geophysics, Geosystems, v. 4, 8407, doi:10.1029/2003GC000559.

Boltovskoy, E., Giussani, G., Watanabe, S., and Wright, R., 1980, Atlas of benthic shelf foraminifera of the southwest Atlantic: The Hague, Dr W. Junk bv Publishers, 154 p.

Broecker, W.S., Sutherland, S., and Smethie, W., 1995, Oceanic radiocarbon: Separation of the natural and bomb components: Global Biogeochemical Cycles, v. 9, p. 263-288.

Conkright, M.E., Locarnini, R.A., Garcia, H.E., O'Brien, T.D., Boyer, T.P., Stephens, C., and Antonov, J.I., 2002, World Ocean Atlas 2001: Objective analyses, data statistics, and figures, CD-ROM documentation: Silver Spring, MD, National Oceanographic Data Center, 17 p.

Cox, P.M., 2001, Description of the 'TRIFFID' dynamic global vegetation model: Hadley Centre Technical Note 24, 17 p.

Cox, P.M., Betts, R.A., Bunton, C.B., Essery, R.L.H., Rowntree, P.R., and Smith, J., 1999, The impact of new land surface physics on the GCM simulation of climate and climate sensitivity: Climate Dynamics, v. 15, p. 183-203.

Crowley, T.C., 1992, North Atlantic Deep Water cools the Southern Hemisphere: Paleoceanography, v. 7, p. 489-497.

Ewing, M., and Lonardi, A.G., 1971, Sediment transport and distribution in the Argentine Basin. 5. Sedimentary structure of the Argentine margin, basin and related provinces, *in* Ahrens, L.H., Press, F., Runcorn, S.K., and Urey, H.C., eds., Physics and Chemistry of the Earth: Oxford, Pergamon, v. 8, p. 123-251.

Fairbanks, R.G., 1989, A 17,000-year glacio-eustatic sea level record: influence of glacial melting rates on Younger Dryas event and deep-ocean circulation: Nature, v. 342, p. 637-642.

Hibler, W.D., 1979, A dynamic-thermodynamic sea-ice model: Journal of Physical Oceanography, v. 9, p. 815-846.

Hubbard, A., Hein, A.S., Kaplan, M.R., Hulton, N.R.J., and Glasser, N., 2005, A modelling reconstruction of the Last Glacial Maximum ice sheet and its deglaciation in the vicinity of the Northern Patagonian Icefield, South America: Geografiska Annaler Series A, v. 87, p. 375-391.

Hughen, K.A., and 26 others, 2004, Marine04 marine radiocarbon age calibration, 0–26 cal kyr BP: Radiocarbon, v. 46, p. 1059-1086.

Hunke, E.C., and Dukowicz, P.R., 1997, An elastic-viscous-plastic model for sea ice dynamics: Journal of Physical Oceanography, v. 27, p. 1849-1867.

Kalnay, E., Kanamitsu, M., Kistler, R., Collins, W., Deaven, D., Gandin, L., Iredell, M., Saha, S., White, G., Woolen, J., Zhu, Y., Leetmaa, A., Reynolds, B., Chelliah, M., Ebisuzaki, W., Higgins, W., Janowiak, J., Mo, K.C., Ropelewski, C., Wang, J., Jenne, R., and Joseph, D., 1996,The NCEP/NCAR reanalysis project: Bulletin of the American Meteorological Society, v. 77, p. 437-471.

Knorr, G., and Lohmann, G., 2003, Southern Ocean origin for the resumption of Atlantic thermohaline circulation during deglaciation: Nature, v. 424, p. 532-536.

LeGrande, A.N., and Schmidt, G.A., 2006, Global gridded data set of the oxygen isotopic composition in seawater: Geophysical Research Letters, v. 33, L12604, doi:10.1029/2006GL026011.

Lonardi, A.G., and Ewing, M., 1971, Sediment transport and distribution in the Argentine Basin. 4. Bathymetry of the continental margin, Argentine Basin and other related provinces, canyons and sources of sediments, *in* Ahrens, L.H., Press, F., Runcorn, S.K., and Urey, H.C., eds., Physics and Chemistry of the Earth: Oxford, Pergamon, v. 8, p. 79-121.

Lutze, G., 1986, *Uvigerina* species of the eastern North Atlantic: Utrecht Micropaleontological Bulletins, v. 35, p. 21-46.

Manabe, S., and Stouffer, R.J., 1997, Coupled ocean-atmosphere model response to fresh-water input: Comparison to Younger Dryas event: Paleoceanography, v. 12, p. 321-336.

Meissner, K.J., Weaver, A.J., Matthews, H.D., and Cox, P.M., 2003, The role of land surface dynamics in glacial inception: a study with the UVic Earth System Model: Climate Dynamics v. 21, p. 515-527.

Pacanowski, R.C., 1996, MOM 2. Documentation, user's guide and reference manual: GFDL Ocean Group Technical Report 3.2, 328 p.

Paul, A., and Schäfer-Neth, C., 2004, The Atlantic Ocean at the Last Glacial Maximum: 2. Reconstructing the current systems with a global ocean model, in Wefer, G., Mulitza, S., and Ratmeyer, V., eds., The South Atlantic in the Late Quaternary: Reconstruction of material budgets and current systems: Berlin, Springer-Verlag, p. 549-583.

Reimer, P.J., and 28 others, 2004, IntCal04 terrestrial radiocarbon age calibration, 0-26 cal kyr bp: Radiocarbon, v. 46, p. 1029-1058.

Reimer, P.J., and Reimer, R.W., 2001, A marine reservoir correction database and on-line interface: Radiocarbon, v. 43, p.461-463.

Rühlemann, C., Mulitza, S., Lohmann, G., Paul, A., Prange, M., and Wefer, G., 2004, Intermediate depth warming in the tropical Atlantic related to weakened thermohaline circulation: Combining

paleoclimatic data and modelling results for the last deglaciation: Paleoceanography, v. 19, PA1025, doi:10.1029/2003PA000948.

Semtner, A.J., 1976, A model for the thermodynamic growth of sea ice in numerical investigations of climate: Journal of Physical Oceanography, v. 6, p. 379-389.

Shackleton, N.J., 1974, Attainement of isotopic equilibrium between ocean water and the benthonic foraminifera genus *Uvigerina*: isotopic changes in the ocean during the last glacial: Colloques Internationaux C.N.R.S., v. 219, p.203-209.

Stuiver, M., and Östlund, H.G., 1980, GEOSECS Atlantic radiocarbon: Radiocarbon, v. 22, p. 1-24.

Stuiver, M., and Polach, H.A., 1977, Discussion reporting of ^{14}C data: Radiocarbon, v. 19, p. 355-363.

Stuiver, M., and Reimer, P.J., 1993, Extended ^{14}C database and revised CALIB 3.0 ^{14}C age calibration program: Radiocarbon, v. 35, p. 215-230.

Turner, K.J., Fogwell, C.J., McCulloch, R.D., and Sugden, D.E., 2005, Deglaciation of the eastern flank of the NPI and associated continental-scale lake diversions: Geografiska Annaler Series A, v.87, p. 363-374.

Weaver, A.J., Eby, M., Wiebe, E.C., Bitz, C.M., Duffy, P.B., Ewen, T.L., Fanning, A.F., Holland, M.M., MacFadyen, A., Matthews, H.D., Meissner, K.J., Saenko, O., Schmittner, A., Wang, H., and Yoshimori, M., 2001, The UVic Earth System Climate Model: Model description, climatology, and applications to past, present and future climates: Atmosphere-Ocean, v. 39, p. 361-428.

Weaver, A.J., Saenko, O.A., Clark, P.U., and Mitrovica, J.X., 2003, Meltwater pulse 1A from Antarctica as a trigger of the Bølling-Allerød warm interval: Science, v. 299, p. 1709-1713.

Yokoyama, Y., Lambeck, K., De Deckker, P., Johnston, P., and Fifield L.K., 2000, Timing of the Last Glacial Maximum from observed sea-level minima: Nature, v. 406, p. 713-716.